Physics in Medicine & Biology

PAPER • **OPEN ACCESS**

A flexible 8.5 MHz litz wire receive array for field-cycling imaging

To cite this article: Robert S Stormont *et al* 2023 *Phys. Med. Biol.* **68** 055016

IOP Publishing Phys. Med. Biol. 68 (2023) 055016 https://doi.org/10.1088/1361-6560/acb9d0

Physics in Medicine & Biology

IPEM Institute of Physics and Engineering in Medicine

OPEN ACCESS

RECEIVED
15 August 2022

REVISED
2 February 2023

ACCEPTED FOR PUBLICATION
7 February 2023

PUBLISHED
27 February 2023

PAPER

A flexible 8.5 MHz litz wire receive array for field-cycling imaging

Robert S Stormont[1,2,*], **Gareth R Davies**[1], **P James Ross**[1], **David J Lurie**[1] **and Lionel M Broche**[1]

[1] Aberdeen Biomedical Imaging Centre, School of Medicine, Medical Sciences & Nutrition, University of Aberdeen, Aberdeen AB25 2ZD, United Kingdom

[2] GE Healthcare, 3200 N Grandview Blvd, Waukesha, WI, United States of America

[*] Author to whom any correspondence should be addressed.

E-mail: robert.stormont@abdn.ac.uk

Keywords: RF Coil, array, low-field, noise figure, signal-to-noise, litz, flexible

Supplementary material for this article is available online

Abstract

Objectives. Low frequency coils present unique challenges as loop losses, component losses, and the supporting electronics can significantly degrade the signal-to-noise ratio (SNR). SNR may already be a limiting factor with MRI at low field (and frequency), therefore the minimization of additional loss is particularly important. If interactions between loops are managed, array coils can provide increased SNR, coverage, and potentially imaging speed. In this work, we investigate methods to characterise and preserve SNR from a low frequency coil array, allowing a more geometrically conforming array for quick, no-tune application with various anatomies. *Approach*. Single and multi-turn, 16.2 cm diameter litz wire loops were constructed and characterised for losses under various loading conditions. Low noise preamplifiers were acquired and characterized, as well as interfacing electronics were developed and evaluated. A bench level SNR test was implemented to observe the effects of tuning and loading on individual coils. The results were used to select a design for construction of a 6-channel, flex array coil. *Main results*. Ultra fine strand litz wire exhibited lower losses than equivalent diameter solid wire which should translate to improved SNR and provides the mechanical flexibility needed in a conforming array. Single turn loop losses were dominant under all loading conditions; however, 2 and 3 turn loops were body loss dominated under modest loading conditions. Preamplifier blocking achieved was well short of our design goal and critical overlaps became necessary for coil-to-coil interaction control. Our finished array, a 3-channel posterior array coil and a 3-channel anterior array coil, conforms nicely to various anatomies and is providing consistent results in various volunteer study trials. *Significance*. Receive coils are challenging at low fields as loop losses often limit the final SNR. This is exacerbated in an array coil as loops may be smaller and not coupled well to the body. In this work we have demonstrated that body loss dominance is possible with 16.2 cm loops at 8.5 MHz. We have optimized, built, and tested low noise interfacing electronics and characterized the SNR penalties as the tuning and loading is varied, a key parameter in a geometrically flexible array designed for rapid setup. The resultant 6-channel, general-purpose array is supporting various Field-Cycling Imaging studies where body habitus and anatomies require a flexible, adaptable array coil which can be quickly positioned and utilized.

1. Introduction

Field-Cycling Imaging (FCI), also known as Fast Field-Cycling Magnetic Resonance Imaging (FFC-MRI), is an approach which can measure NMR parameters such as T_1 as a function of B_0 (T_1 dispersion), a potential biomarker in various pathologies (Lurie *et al* 2010). The main magnetic field is driven over a range of values, as opposed to the fixed field utilised in a conventional MRI system and may be driven to its highest value for signal detection as the higher value can yield a higher Signal-to-Noise Ratio (SNR). One FCI system being developed

and studied at the University of Aberdeen (Broche *et al* 2019) has a solenoidal configuration that can switch a whole-body accommodating B_0 field from 0 to 0.2 T in 12 ms. Signal detection is generally acquired at about 0.2 T, with hydrogen protons resonating at approximately 8.5 MHz, and the detection coil oriented to capture the transverse fields. 0.2 T is a modest field for signal readout, and the SNR of detected signals is reduced relative to typical 1.5 T or 3.0 T fixed-field systems (Hoult and Richards 2011). Additionally, detecting and preserving that SNR can be a challenge as losses in the loop conductor, interface components, and protection circuitry can be significant relative to the body losses.

Studies are underway in our laboratory, measuring relaxation signatures of various healthy and diseased tissues (UK Stroke Forum Abstracts 2018, Broche *et al* 2019). To date, they have been conducted with single channel transmit/receive (Tx/Rx) coils for head, knee, and breast, each coil requiring careful tuning per volunteer to optimise performance. We are now optimising a whole-body transmit subsystem and low-noise, multi-channel receive subsystem to support receive-only arrays and to allow volunteer imaging of the colon, heart, liver, and kidneys. A torso-conforming array is being developed which is expected to provide improved SNR when compared to a body-accommodating volume coil (Roemer *et al* 1990). The further goal of this study is to design an array that is quick to apply, without the need for patient-to-patient adjustments (tuning and matching), to reduce the scan set-up time.

Throughout this paper, the term 'loop' is used to describe an area encompassing conductor (as well as the conductor with the proper capacitor(s) to counter its inductive reactance); the term 'coil' is used to describe a loop that is interfaced to a preamplifier; and the term 'array' or 'coil array' to denote more than a single coil in a geometric arrangement. Additionally, 'loop losses' are those inherent in the loop conductors when a loop is 'unloaded', and 'body losses' describe the additional loss from having the loop loaded in proximity to a lossy body. When specifically talking about our testing method where the lossy body is a saline solution vessel, the term 'phantom losses' is used.

Loop losses are a particular challenge at low fields (Redpath 1998, Gilbert *et al* 2008). Ensuring body losses markedly dominate the loop losses is a major focus of our design effort. Because we are seeking a highly flexible, conforming array, large diameter conductors are unattractive and other technologies were considered. One method to reduce the losses in conductors is to cool conventional conductors or to employ superconductors operating at low temperatures. Losses can be exceptionally low, and coils have been investigated which have losses more than an order of magnitude lower than conventional coils (Bracanovic *et al* 2001, Ma *et al* 2003). However, with a high-temperature superconductor, the coil must be contained in a liquid nitrogen cryostat which can force the element away from the anatomy of interest. Also, the low temperatures can be a safety issue for the patient, and the cool-down time could add set-up delays. Additionally, the extremely low loss of the coil demands precise tuning and matching and can impart frequency-related shading to an image and excessively long ringing after excitation has ended. For these reasons, cryogenic coils were not investigated in this work and instead we focused on the following aspects, described below.

1.1. Skin effect and Litz wire

The skin effect is the tendency for high-frequency ac currents to flow on the surface of a conductor and is a natural consequence of Maxwell's equations (Terman 1943, Landau and Lifshitz 1984). As a result, the current-carrying cross-section of a wire can be greatly reduced at high frequency, leading to a larger electrical resistance than what one expects at dc. The skin depth, δ, is the radial distance d into the conductor in which the current density J has reduced to 1/e (about 37%) of its value at the surface ($J_d \approx J_{surface} e^{-d/\delta}$) and at 8.5 MHz in copper, δ is about 22 μm.

An established method that is utilised to reduce conductor losses at lower frequencies is the application of litz wire. Litz wire is an assembly of fine wires with, for maximum benefit, diameters less than a skin depth and insulated from one another to form a conductive bundle. This arrangement can cause the current to flow in a larger cross-section area than in a solid single conductor, thus lowering the losses. The early classic literature on litz wire indicates a usefulness up to approximately 3 MHz where skin-depth and proximity effects then diminish the value of the litz wire approach (Reese *et al* 2018). However, development of ultra-fine litz wire constructions may extend benefits to 10 MHz and higher (Giovannetti and Menichetti 2017, Russell and Carter 2019). Giovannetti has surveyed the use of litz wire in MRI coils showing successes from 100 s of kHz and into the several MHz range (Grafendorfer *et al* 2006). Recent experiments and modeling of low-frequency MRI coils with 0.032 mm and 0.02 mm litz strand bundles show significant loss improvements up to 5.7 MHz, and predict a nearly 50% reduction in loss of a 2.0 mm outer diameter bundle of 0.02 mm strands versus a solid copper wire of the same diameter and length at 8.5 MHz (Smith 1972).

1.2. Multi-turns

A multi-turn loop can benefit situations where body losses do not significantly dominate the loop losses. Given a fixed conductor dimension and area, loop losses should increase proportional to N (N being the number of

turns), while body losses increase as N^2. However, the proximity effect crowds current into adjacent conductors and causes the losses to rise faster than ideal, diminishing a multi-turn loop's value (Pettai 1984, Giovannetti 2014). Another potential challenge with a multi-turn coil could include an increasing mutual inductance between loops, which is expected to increase as N^2 for equivalent geometries and place more demand on coil-to-coil decoupling performance.

1.3. Preamplifier

Preamplifiers in MR systems are used to overcome noise from ensuing stages of the MRI system receive chain, and should reduce SNR by a minimal amount, or equivalently exhibit a low Noise figure (*NF*). *NF* is the ratio of the output signal power to noise power to the input signal power to noise power of a network (Roemer *et al* 1990).

1.4. Decoupling

With the advent of coil arrays, the preamplifier has also become a crucial component in the control of interactions by restricting loop current flow and lowering the effects of inductive mutual coupling (Lee *et al* 2002). Since our array is intended to be flexible, and mutual inductance between loops will vary with placement and geometry, our approach is to rely heavily on preamplifier blocking (decoupling) to reduce coil-to-coil interaction.

Other methods to control the mutual inductance between loops such as the strategic introduction of inductive or capacitive transformers may be employed (Lee *et al* 2002), however a very flexible coil with varying mutual inductance between loops may not have a single solution, and anterior to posterior coil coupling may not readily be addressed this way.

2. Materials and methods

2.1. Design inputs

Our intention was to create an array consisting of an anterior portion and *a posterior* portion which would work in conjunction to provide a 30 cm diameter spherical field-of-view (FOV) and provide adequate SNR to typical torso anatomy depths. An earlier laboratory prototype had loops areas of approximately 206 cm^2 (equivalent to a 16.2 cm diameter circle) and we maintained that loop size in our study. Arrangements of 3 to 4 loops of this size in both the anterior and posterior portions of the array were expected to give us the desired FOV.

While other element sizes, shapes, and channel counts may prove superior for some conditions, we chose to focus on a given loop size for our study and array. The 16.2 cm loops allow us to examine conductor losses and evaluate the performance of low noise electronics under variable conditions while providing good coverage for many torso applications.

A 1600 × 0.020 mm litz wire bundle with diameter ~1.5 mm (Elektrisola Co. Reichshof-Eckenhagen, Germany) was compared with a solid copper wire of 1.7 mm diameter. Single turn, 16.2 cm diameter loops were constructed and resonated with the required high Q ATC C-series capacitor (ATC corporation, Huntington Station, NY. USA).

2.2. Decoupling performance

Due to mutual inductance between loops, current in one loop develops an *EMF* in the magnetically coupled loop. The exact loop geometries and overlaps determine the mutual inductance between loops and will be variable in a flexible coil. Also, the anterior and posterior loops are expected to reside coaxial to each other at varying distances and varying coupling. Limiting current in the loops can lower the polluting *EMF* induced in a magnetically coupled loop.

Referring to figure 1(a), V_a and V_b are the *EMF*s induced (and driving current in) loops 1 and 2 respectively. If we want the polluting signal from loop 2's induced *EMF*, V_b, to be less than 10% at loop 1, then $V_b j\omega kL/(R_2 + Z_2) < V_b 0.1$, and, with $R_2 \ll Z_2$ then

$$Z_2 > \frac{k_m \omega L}{0.1} \text{or } k_m < \frac{0.1 Z_2}{\omega L}, \tag{1}$$

where ω is the operating frequency in radians per second, L is the loop inductance, R_2 is the conductor and body losses in loop 2. Z_2 is the blocking impedance at loop 2, and k_m is the magnetic coupling coefficient between loops. This assumes that the coupling between loops is solely through their mutual inductance; other mechanisms such as electric field and local eddy current coupling could also be significant (Kumar *et al* 2009).

In our approach, our loops are tuned on resonance to a real impedance, and this applies to the preamplifiers input as well. The real input impedance of the preamplifier is matched to a real impedance at the loop (the

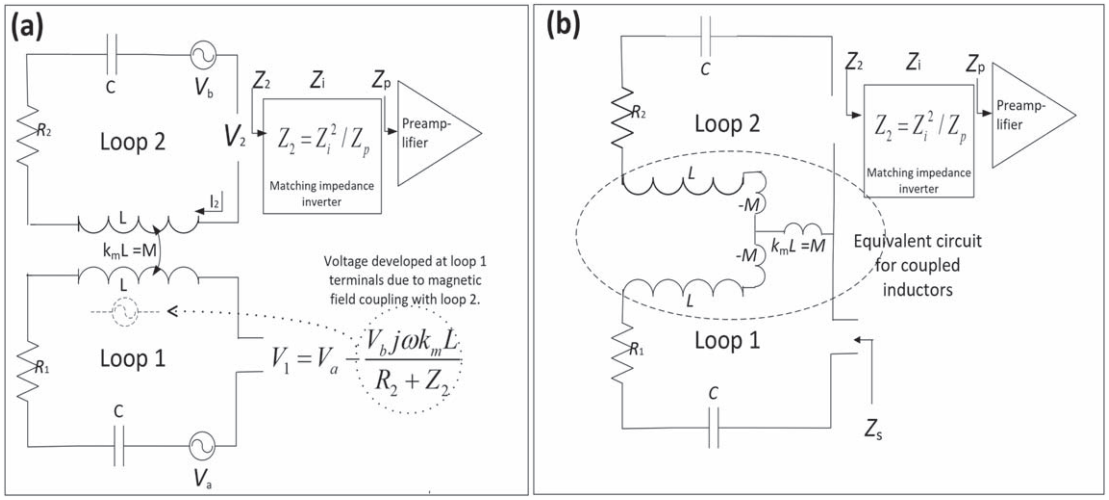

Figure 1. (a) Circuit model of magnetically coupled loops and impact of blocking impedance where L is the loop inductance; C is the tuning capacitance $= (1/\omega^2 L)$; R_1, R_2 are the conductor and body losses in loops 1 and 2; V_2 is the voltage at loop 2 s terminals; V_a, V_b are the *EMF*s induced into loops 1 and 2; Z_p = preamplifier input impedance; Zi = impedance inverter characteristic value; Z_2 = the blocking impedance at loop 2. I_2 is the current established in loop 2 due to V_b; V_1 is the voltage established at loop 1 including coupling from loop 2 when its preamp and matching are disconnected ; k_m is the magnetic coupling coefficient between loops; M is the mutual inductance between loops (k_mL). (b) An equivalent circuit for the mutual inductance with Z_s being the impedance looking into loop 1 with its preamp and matching disconnected.

blocking or decoupling impedance to limit current in the loop). This real blocking impedance, via the loop-to-loop mutual inductance, adds an additional resistive loss term to an array loop and lower its unloaded Q (Sánchez-Heredia *et al* 2019). Figure 1(b) is an equivalent circuit of the mutual inductance (Izadian 2019) depicted in figure 1(a), revealing the additional loss. By opening and looking into loop 1 in our equivalent circuit model shown in figure 1(b), we see that:

$$Z_S = R_1 - jZ_C + jZ_L - j\omega M + \frac{j\omega M(R_2 - jZ_C + jZ_L - j\omega M + Z_2)}{j\omega M + R_2 - jZ_C + jZ_L - j\omega M + Z_2} \tag{2}$$

with Z_C and Z_L equal (tuned condition), $R_2 \ll Z_2$, and $M = k_mL$.

Z_S now simplifies to an all-real impedance of

$$Z_S = R_1 + \frac{(k_m\omega L)^2}{Z_2} = R_{Total}. \tag{3}$$

In addition to its conductive and body losses R_1, there is an additional loss term $(k_m\omega L)^2/Z_2$. This is evident as a reduction of the Q of the loop being interfered with. With our noise increasing proportionally to the square root of the total loop resistance we can calculate a SNR penalty.

For a 10% noise penalty, $\sqrt{R_{Total}/R_1} = 1.1$, requiring that:

$$Z_2 > \frac{(k_m\omega L)^2}{0.21R_1} \text{or } k_m < \frac{\sqrt{0.21R_1Z_2}}{\omega L}. \tag{4}$$

Note that in this example, k_m is the coupling between two coils, and in a higher element count arrays, all will couple to some degree. For simplification, we are considering k_m as an aggregate of the various magnetic coupling coefficients. Please see Supplemental Materials for the development of a resistive noise coupling model of an example 4-channel coil array.

This noise coupling may prove to be a more demanding blocking requirement than that required to keep the signal coupling below 10%, depending on the loop inductance, magnetic coupling, and loading. Figure 2 presents modeled results of circular, co-planar coil magnetic coupling coefficients, coaxial loop magnetic coupling coefficients (Rosa and Grover 1916) and includes some highlighted overlap/underlap and separation regions.

2.3. Preamplifier

We acquired two preamplifiers for evaluation in this study from WanTcom Inc., Chanhassen, MN, USA . The WMA0HA is a complete amplifier and the WMA08HB has nodes brought to outside so that low loss matching components can be used.

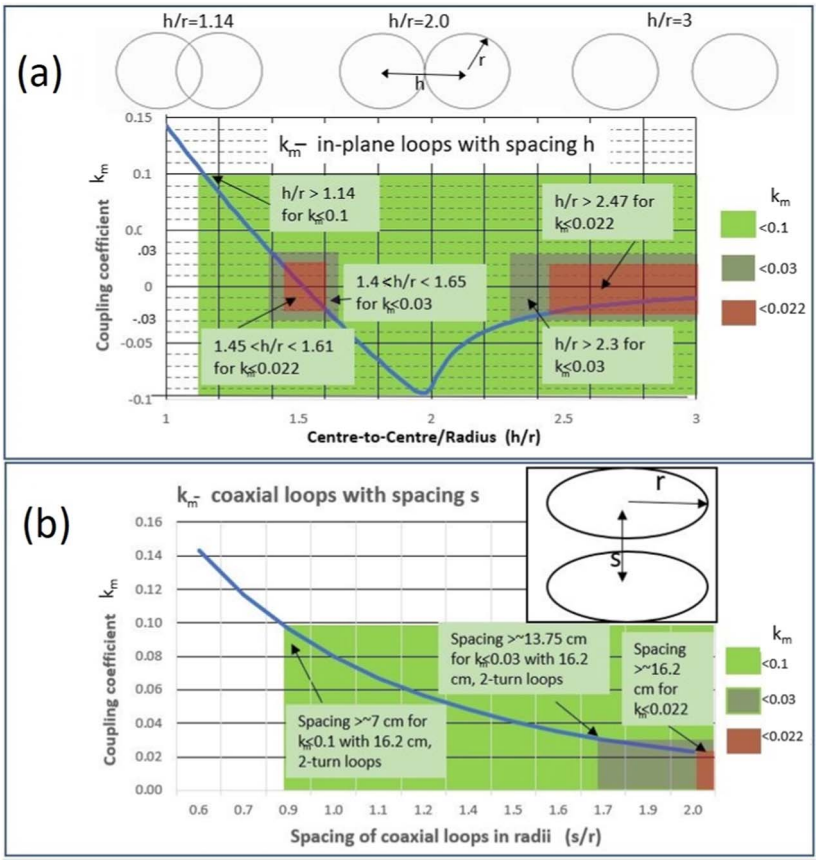

Figure 2. (a) A Biot–Savart wire model for coplanar loops, outlining the overlap region that prevent the magnetic coupling coefficient, k_m, from exceeding 0.1, 0.03, and 0.022. (b) Maxwell's model ((Rosa 1916) for coaxial loops and indicating the spacing required to keep the magnetic coupling coefficient below 0.1, 0.03, and 0.022.

The preamplifier's noise contribution (or the degradation of the SNR as the signal and noise depends on the preamplifier) depends on the source impedance which is feeding it. Here we utilize a semiconductor industry standard where a device's noise parameters allow calculation of its noise factor F (Noise figure (NF) = 10 log(F)) given the source impedance feeding it, Γ_{src}. The noise parameters provided include the term r_{n}, a normalised noise resistance of the device, F_{min}, the minimum attainable noise factor of the device and Γ_{opt}, the required source impedance to achieve F_{min} (Gonzalez 1996). The NF(dB) is then

$$NF\,(dB) = 10\log\left(F_{\mathrm{min}} + 4r_n\frac{|\Gamma_{src} - \Gamma_{opt}|^2}{((1 - |\Gamma_{src}|)^2(|1 + \Gamma_{opt}|^2))}\right). \tag{5}$$

A convenient way of viewing NF is depicted in figure 3, mapping the locus of source reflection coefficients for a particular NF onto a Smith chart. The goal is to reach the optimum source impedance for best NF under varying load and tuning conditions. The WanTcom preamplifiers were specified to have a low input impedance of 1.5–2.0 Ω, a high optimum source impedance of 150 Ω and 28 dB of gain with a 150 Ω source. The relatively low input impedance and high optimum source impedance both directly impact the achievable preamplifier blocking impedance.

2.4. Matching

Loaded tests with a 2-turn, 16.2 cm loop indicated that light loads present about 0.35 Ω at the loop terminals, and that heavy loading approaches 1.0 Ω. It is desirable to select a matching circuit that converts those resistances to a preamplifier source impedance that maintains a NF ⩽1 dB, while simultaneously converting an expected preamplifier input impedance of ⩽2.0 Ω to the preamp blocking impedance.

A 2 Ω preamplifier, with a 14 Ω impedance inverter would yield a blocking impedance of $14^2/2 = 98$ Ω. This same converter would translate a 0.35 Ω loop to $14^2/0.35 = 560$ Ω. From equation (5), the preamplifier would exhibit a 1.08 dB NF with this source impedance and improve as coil loading increases.

A lattice balun was used as the impedance inverter to prevent common mode current from body coil electric fields and to match the preamplifier and loop (Bakalski *et al* 2002). If there is no common mode or loop-to-loop

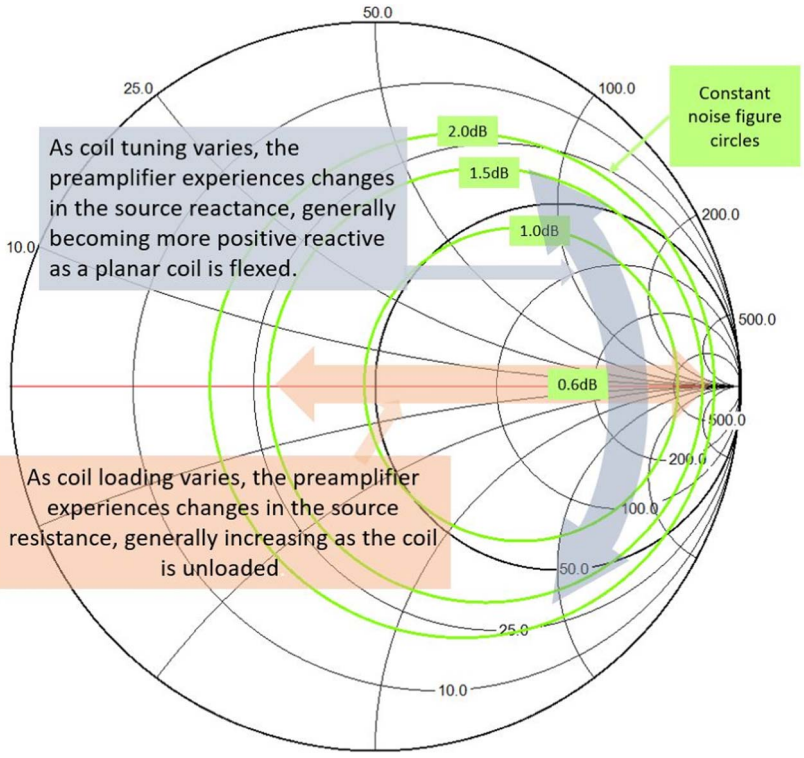

Figure 3. Example of Noise figure circles for a preamplifier (WMA08HA preamplifier with noise parameters: ($NF_{\min} = 0.60dB$, $\Gamma_{opt} = 0.52$, $r_n = 0.21\ \Omega$)), with annotations of typical loading and tuning effects.

current concerns, a quarter wave pi section of the same characteristic impedance as the lattice can be utilized, resulting in the same blocking and source impedances.

3. Evaluation methods

3.1. Loop loss characterization

Loop losses were evaluated over varying load conditions by series resonating the loop and measuring the loaded and unloaded Q values. Assuming the body losses are due only to the non-conservative electric fields in the sample volume, we could then calculate the penalised SNR (%SNR) when compared to an identically dimensioned and positioned lossless loop. Kumar and Edelstein documented the use of the Q ratio to describe the SNR lost (a coil's Noise figure) due to coil losses, R_{coil}, relative to body losses, R_{body} as follows (Kumar *et al* 2009), Q can be expressed as the ratio of the coil loop's reactance, ωL, to the losses from the loop, R_{coil}, or loop and body, $R_{coil} + R_{body}$, $Q_{unloaded} = \frac{\omega L}{R_{coil}}$ and $Q_{loaded} = \frac{\omega L}{R_{coil} + R_{body}}$. The available SNR, with losses just from body is

$$SNR = \frac{EMF}{\sqrt{4kTBR_{body}}} \tag{6}$$

and the reduced SNR when coil losses are added is

$$SNR_{w/coillosses} = \frac{EMF}{\sqrt{4kTB(R_{coil} + R_{body})}} \tag{7}$$

and then when substituting Q_{loaded} and $Q_{unloaded}$ into equations (6) and (7) yields

$$\%SNR = \frac{SNR_{w/coillosses}}{SNR} = \sqrt{1 - \frac{Q_{loaded}}{Q_{unloaded}}}\,(100), \tag{8}$$

where k = Boltzmann's constant, T = temperature in degrees Kelvin, B = bandwidth in Hz.

This method assumes that the magnetic flux generating the *EMF* and the body losses are from the same volume. Body losses are not desired, but they are inevitable given that the coil is coupled to a conductive region from which the signal B field emanates. At extremely low fields and/or with small elements, coil losses may almost exclusively determine the noise, and the coils are described as operating well into the coil noise

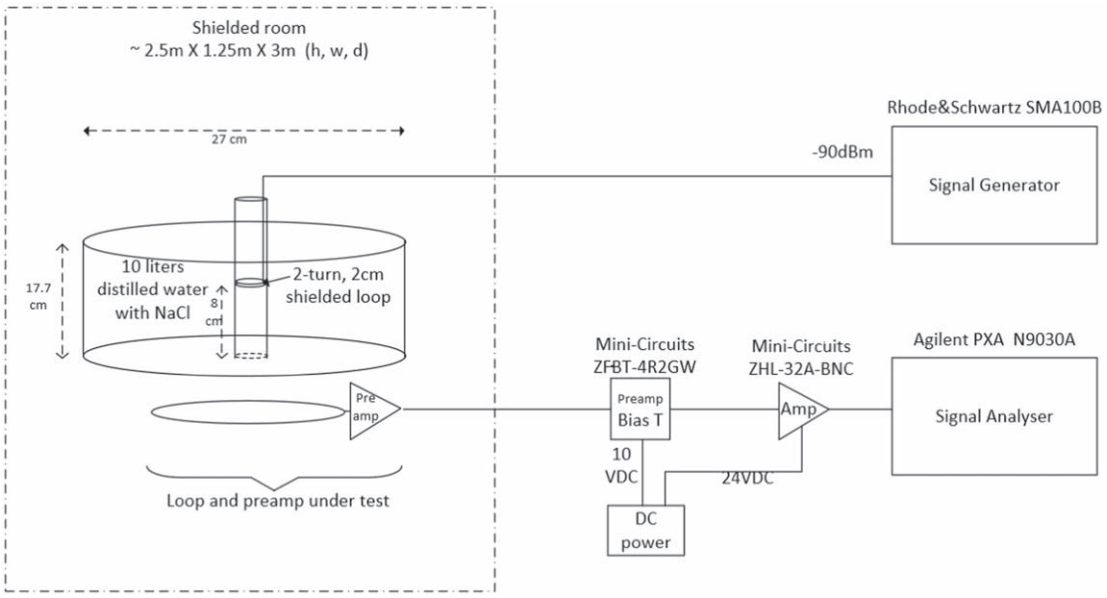

Figure 4. SNR test rig showing the loop and preamplifier under test placed 1 cm below a cylindrical tank containing distilled water with various concentrations of NaCl to simulate different loading conditions. Signal stimulation is via a 2 cm loop, offset 8 cm above the vessel floor and driven by a −90 dBm source. Signal reception and measurement is performed with a precision signal analyser preceded by a 27 dB gain stage.

dominated (>30% SNR reduction to loop losses) region (Gilbert *et al* 2008). Body losses still exist but can become insignificant relative to the coil losses and the SNR now varies approximately proportional to $1/\sqrt{R_{coil}}$.

To improve loop losses and raise Q_{unloaded}, fine stranded litz wire was compared and selected versus a solid wire. In addition to the potential for reduced losses, fine stranded litz is very flexible and supports a close-fitting array. The ultimate losses in a litz bundle are very complex, well beyond just the smaller strand diameter described as enabling benefit at 8.5 MHz and above (Sullivan 1999). It should be noted that we have not studied or contributed to the development of litz bundles as a part of this project and are relying on the wire supplier's expertise.

3.2. Loop deformation analysis

Deformation of the loops is expected with a conforming array and the coil's resonant frequency is expected to rise when the coil is flexed. To emulate a flexed coil, a resonant loop was wrapped around an 18 cm diameter non-conducting cylinder and a resonant frequency shift of 70 kHz was measured, corresponding to a lowering of the loop inductance by about 2%. This flexure may be similar to wrapping a coil onto a patient's side. The coil then presents a capacitive reactance to the matching circuit that is inverted to an inductive reactance at the preamplifier. We analyse the impact of this loop reactance change on the preamplifier's Noise figure.

3.3. SNR characterisation

An SNR test rig was created which attempts to look at the relative SNR between several of the loop/electronics arrangements. The apparatus has a vessel to hold 10 litres of conductive solution, with a centered, 2 cm tube to insert a test loop probe. Figure 4 is a block diagram of the complete SNR test arrangement which presents the test equipment utilized and a shielded room environment. The added gain block, in addition to the preamplifier gain, ensures the measured noise power is well above the −149 dBm Hz^{-1} noise floor of the signal analyser.

The aim was to create an SNR test that can measure relative changes between different loops, tuning conditions, etc without the need to use an MRI system. The signal is determined by the magnetic flux density produced by the test probe and captured by the axially placed loop, and those geometries are held for each loop and load test. The noise is determined by the source impedance presented to the preamplifier (loaded loop noise plus the input referred Noise figure generated by the preamp for that condition). Both signal and noise are elevated by the preamplifier gain (variable with source impedance) and test equipment gain before measurement and should not affect the SNR. The test has a slight bias over frequency, with the induced *EMF* from the probe changing linearly with frequency. For example, a 0.1 dB reduction when testing at 8.4 MHz versus 8.5 MHz. Additionally, there is a slight bias of less than 0.01 dB over this frequency range which would include cabling, booster amplifier performance, and signal generator level.

Under various loading conditions and frequencies, with the de-energised probe set at 8.0 cm above the vessel bottom, noise power (dBm/Hz) was measured at 8.4 MHz, 8.5 MHz, and 8.6 MHz. The small probe was then energised at 8.4 MHz, 8.5 MHz, and 8.6 MHz, −90 dBm signal, and peak power of the signal out of the coil was measured. SNR for this test is the ratio of that output power to the measured noise power per hertz. Testing at frequencies above and below 8.5 MHz is intended to observe the effects of reactive sources on the preamplifier, without perturbing the coil positioning, tuning, or matching. At 8.5 MHz, a 100 kHz change in frequency represents about a 2% loop reactance mistune, inductive (8.6 MHz) or capacitive (8.4 MHz) that the preamplifier will see. An assertion of the preamplifier supplier (and a major assumption with this test method) is that the preamplifier noise parameters are consistent over these small frequency changes. For comparison purposes a 2% additional capacitance was also added to the coil tuning capacitor and the SNR measurements were retaken at 8.5 MHz.

Various solutions of sodium chloride in distilled water were used to create unloaded (~0.0 g l^{-1}), lightly loaded (~0.2 g l^{-1}), moderately loaded (~1.6 g l^{-1}), and heavily loaded (~3.1 g l^{-1}) conditions. Conductivity of the solutions was measured using a conductivity meter (Myron L Company, Carlsbad, CA 92010 − 7226 USA; model Ultrameter-4P) and the concentration of NaCl was adjusted to attain 0.687 S m^{-1} to represent muscle tissue, 0.358 S m^{-1} to represent liver tissue, and 0.049 S m^{-1} to represent a lightly loaded condition (fat) (Kato *et al* 2005). Unloaded Q values were measured with distilled water only. The loops were placed 1.0 cm below the phantom vessel and Q values were measured with a 2-turn, 2 cm test loop placed centrally, 8 cm above the loop, and a 3 cm test loop placed in plane with the loop, offset by 4 cm outside the loop edge.

The referenced conductivities were measured at 64 MHz, and it is noted that tissue conductivity is frequency dependent and conductivities could be overstated for 8.5 MHz (Gabriel *et al* 1996). However, checks of 2-turn loops loading on the first author's abdomen and chest, with a 1.0 cm spacer, yielded coil losses from 0.75 to 1.0 Ω at 8.5 MHz which is in good agreement with the test rig's measured values when moderate and heavily loaded solutions are tested (0.64 to 0.95 Ω, see results section).

4. Results

4.1. Individual loops

Our purpose in this section was to measure the Q of various wires and turn counts under unloaded and loaded conditions and calculate the expected SNR penalty that arises from loops with finite losses. Additionally, litz wire losses are compared to solid wire losses.

The solid wire loop inductance was calculated to be 500 nH based on the required resonating capacitor, while the litz wire coil was calculated to be 547 nH. Unloaded Q values were measured as 270 for the solid wire and 342 for the litz wire loop. This infers a 15% improvement in loop losses using the litz wire bundle versus the solid wire.

The 16.2 cm loops were constructed with various turn counts, all utilizing the litz bundle. The loops were resonated at 8.5 MHz with a single capacitor and trimmer since, at 3 turns, the length of the loop ($3 \times \pi \times 16.2$ cm ~ 1.5 m) was shorter than 0.1 λ (~3.5 m @ 8.5 MHz) and considered adequate for conservative electric field control (Vaughan and Griffiths 2012). The Q measurements were repeated three times with loop and probes repositioned each time. Loop reactance was calculated from the required resonating capacitor. The Q data allowed calculation of the loop losses (unloaded), loop + phantom losses, and Q ratios and is captured in table 1. The average values were used in subsequent charts and calculations. From the Q data, the %SNR was calculated from equation (8) for each loop and load and is presented in figure 5. The data indicates that ⩾80% of the SNR of a lossless loop is retained for medium and heavy loading with the two- and three-turn loops.

4.2. Interface electronics and preamplifier

In this section, we evaluate the interfacing electronics and preamplifier and determine the blocking impedances provided to the loop.

The preamplifier, loop tuning capacitor, matching impedance inverter, and transmit decoupling diode switch are located on a 5.5 cm × 5.5 cm feed-board, a simplified schematic of which is shown in figure 6(a) (a complete schematic can be found in Supplemental Materials). We limited the number of large inductors and shared functions where possible. RF capacitors were ATC 100 C ceramic series (American Technical Ceramics, NY 11746 USA) with Q values exceeding 1000 at 8.5 MHz. The lattice inductors were Coilcraft 2014VS series (Coilcraft, Illinois 60013 USA) with a Q of approximately 75. The WMA08HA is a complete preamplifier, its noise parameter data was provided by the supplier ($NF_{min} = 0.6dB$, $r_n = 0.21\Omega$, $\Gamma_{opt} = 0.52 < 1$) and it exhibited a typical input impedance of 4.8–5.0 Ω, yielding a measured, modest blocking impedance of 37 Ω when inverted with the lattice balun.

Table 1. Calculated reactance/resistance, and measured *Q* data of unloaded 1, 2 and 3 turn loops. Measured *Q* and calculated *Q* ratios and loop resistances for light, medium, and heavy loaded conditions. **C_r** is the capacitance required to resonate the loop at 8.5 MHz (pF) , **Z** is the calculated loop reactance (jΩ), **L** is the calculated loop inductance (nH), **Q_u** is the measured *Q* unloaded with Average (Ave) and std dev (σ) data, **R_u** is the calculated unloaded loop resistance (Ω), **Q_{ll}** is the measured *Q* when lightly loaded with Average (Ave) and std dev (σ) data, **QR light** is the *Q* ratio—unloaded to light load, **R_{ll}** is the calculated lightly loaded resistance (Ω), **Q_m**is the measured *Q* when medium loaded with Average (Ave) and std dev (σ) data, **QR medium** is the *Q* ratio—unloaded to medium load, **R_m** is the calculated lightly loaded resistance (Ω), **Q_h** is the measured *Q* when heavy loaded with Average (Ave) and std dev (σ) data, **QR heavy** is the *Q* ratio —unloaded to heavy load, **R_h** is the calculated heavily loaded resistance (Ω).

	C_r (pF)	Z (jΩ)	L (nH)	Q_u	R_u (Ω)	Q_{ll}	QR light	R_{ll} (Ω)	Q_m	QR med-ium	R_m (Ω)	Q_h	QR heavy	R_h (Ω)
1-turn	660	28.4	531	Ave 324 σ 4	0.09	Ave 249 σ 3	1.30	0.11	Ave 160 σ 6	2.03	0.18	Ave 111 σ 3	2.92	0.26
2 -turn	172	108.9	2038	Ave 474 σ 4	0.23	Ave 298 σ 5	1.59	0.37	Ave 170 σ 7	2.79	0.64	Ave 114 σ 4	4.16	0.95
3-turn	80	234.1	4382	Ave 503 σ 3	0.47	Ave 269 σ 3	1.87	0.87	Ave 154 σ 1	3.27	1.52	Ave 101 σ 3	4.98	2.32

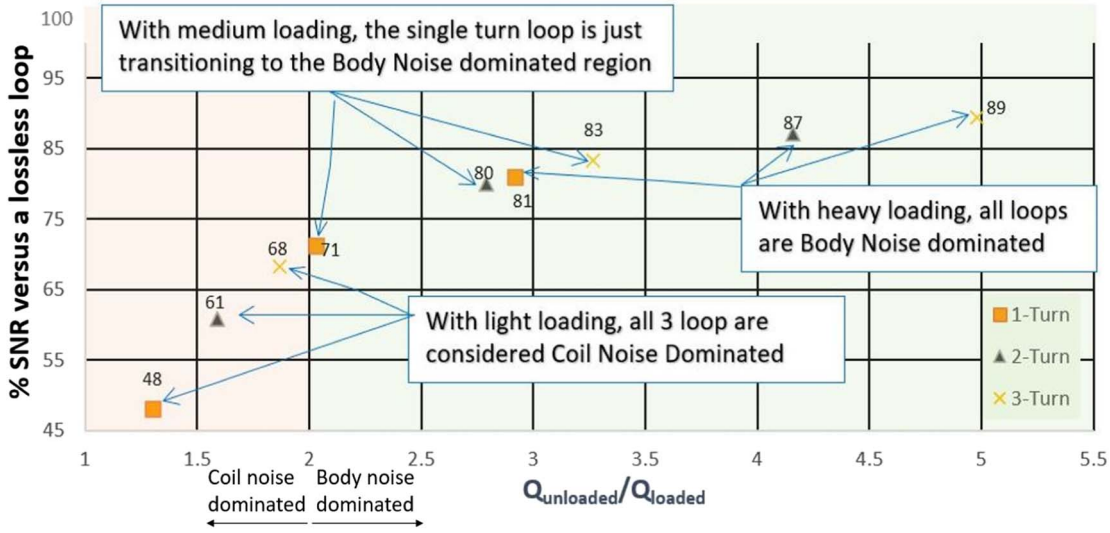

Figure 5. The *%SNR* compared to a lossless loop for the 1, 2, and 3 turn loops based on measured *Q* ratios. Each loops light, medium, and heavy loaded *Q* ratios are included.

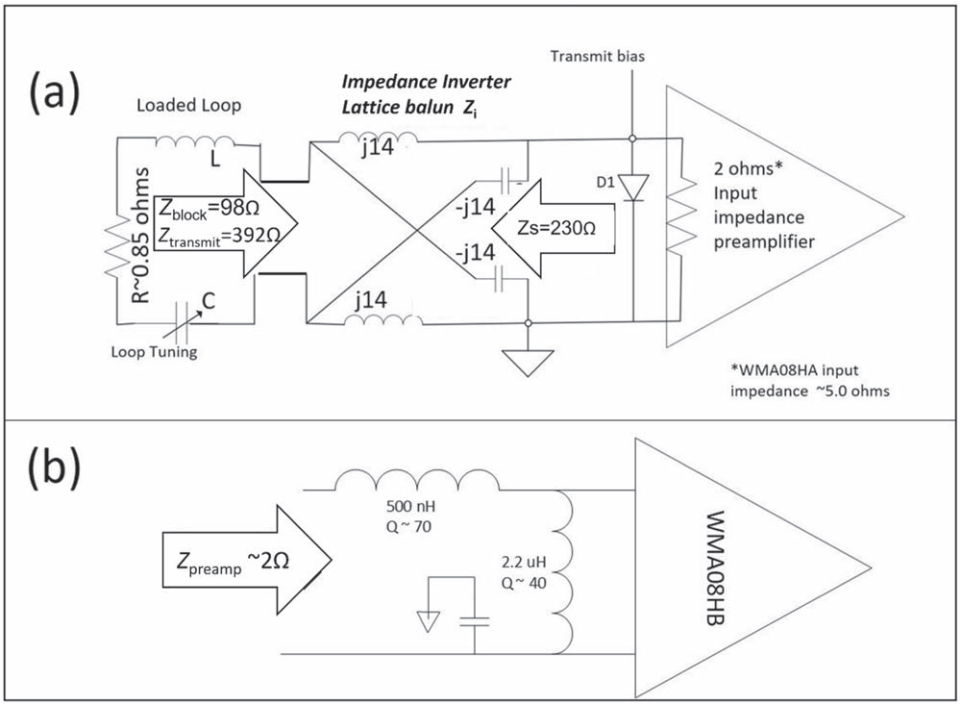

Figure 6. (a) Simplified schematic and typical values describing impedance inverter action between the loop and preamplifier where Z_i = inverter impedance (in this example it is 14 Ω), $Z_{block} = Z_i^2/Z_{preamp}$, $Z_{transmit} = Z_i^2/Z_{D1}$ (in this example D1 on resistance is 0.5 Ω), and $Z_s = Z_i^2/R$. (b) The WMA08HB preamplifier implementation with external inductors to improve input impedance.

The WMA08HB implementation (figure 6(b)) with external, high Q inductors exhibited an input impedance of 2.2 Ω, boosting the preamplifier blocking impedance to a measured 90 Ω. Unfortunately, the WMA08HB design exhibited some instabilities. This may be due to the preamplifier output coupling into the large, external preamplifier input inductors as well as gain peaking increasing as preamplifier blocking increased. Shielding improved the stability, but the inductor *Q* values were reduced by the shield's proximity, making the preamplifier input impedance increase.

Transmit blocking used a DC-biased PIN diode, D1 (Macom, MA, 01851 USA, part MA4P7435), inverted by the same lattice balun as the preamplifier in receive mode (figure 6(a)). A decoupling bias of 120 mA was applied to the interface board and the impedance (transmit blocking) was measured at the loop at approximately 500 Ω.

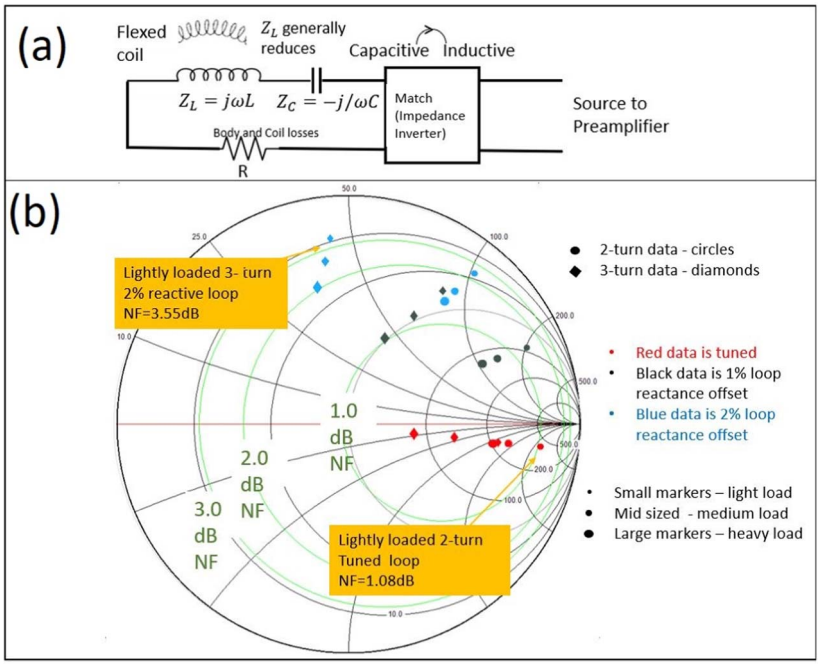

Figure 7. (a) Block diagram depicting the typical lowering of loop inductance with flexure. (b) The data from table 2, placed onto a Smith chart.

4.3. Loop and electronics performance

In this section, we calculate the potential loss in SNR due to the matching and preamplification of the loop under flexing conditions. Additionally, we calculate the potential Noise figure penalties that can occur when loops are deformed.

The two- and three-turn loops were interfaced to the preamplifier via the same feed-board and source impedance was measured under tuned conditions. Figure 7(a) depicts the situation that occurs if a coil loop is flexed. Along with the measured tuned impedances, 1% and 2% loop capacitive reactance offsets were modeled to generate preamplifier-seen source impedances and are captured in table 2. Resulting Noise figure impacts are presented on a Smith chart in figure 7(b). Figure 8 shows the expected SNR loss due to the elevated Noise Figures. When tuned, the preamplifier Noise Figures are ~1 dB or less for both two- and three-turn coils under all loading conditions and degrade significantly when the loop is measured off-frequency, particularly when lightly loaded. In each case, the detuning by addition of a capacitor dropped the SNR when measuring at 8.5 MHz.

4.4. SNR characterisation

Here we directly measured the SNR (power) for the complete coils under various loading conditions, both at the coil operating frequency and off frequency to represent a detuned loop.

The 2- and 3-turn coils' SNR values were evaluated when under light, medium, and heavy loading conditions. The loops were first coarse tuned, unloaded, to provide a real impedance to the preamplifier, then trim-tuned in the test rig by minimizing the noise power output at 8.5 MHz, with the loading phantom filled with distilled water.

Figure 9(a) presents the collected noise power and signal power on the 2-turn and 3-turn coils under light, medium, and heavy loading at frequencies of 8.4 MHz, 8.5 MHz, and 8.6 MHz. Additional data was taken for each loading condition at 8.5 MHz with a 3.6 pF capacitor in parallel with the loop tuning capacitor (approximately 2%).

Figure 9(b) presents the calculated SNR (Signal power (dB)—Noise power (dB)) of the 2-turn and 3-turn coils under light, medium, and heavy loading at frequencies of 8.4 MHz, 8.5 MHz, and 8.6 MHz. Additional data was taken for each loading condition at 8.5 MHz with a 3.6 pF (2-turn loop) and 1.5 pF (3-turn loop) capacitor added parallel with the loop tuning capacitor (approximately 2%). All measurements were repeated 3 times and the average value in each condition is presented in the figures. Scales are maintained at 0.5 dB division^{-1}. In both the two and three turn coils, our highest SNR is when we are on the tuned frequency of 8.5 MHz.

Table 2. 2-turn and 3-turn loop measured reactance data for light loading (0.049 S m^{-1}), medium loading (0.358 S m^{-1}), and heavy loading (0.687 S m^{-1}) with tuned, 1% and 2% capacitive reactance offsets. Calculated results of impedance presented to preamplifier after inversion, and calculated preamp Noise figure with presented impedances.

		Measured loop impedance (Ω)			Calculated inverted impedance (Ω)			Calculated noise figure (dB)		
		Light load	Medium load	Heavy load	Light load	Medium load	Heavy load	Light load	Medium load	Heavy load
2-Turn loop	Tuned	0.37	0.64	0.95	398 - j256	255—j82	206—j57	1.08	0.71	0.65
	1% reactive	0.37- j1.15	0.64 - j1.15	0.95 - j1.15	87 + j204	119 + j139	120 + j109	1.36	0.86	0.77
	2% reactive	0.37 -j2.30	064—j2.30	0.95—j2.30	20 + j103	35 + j93	42 + j86	2.44	1.54	1.31
3-Turn loop	Tuned	0.87	1.52	2.32	223—j61	134—j19	90—j80	0.67	0.62	0.69
	1% reactive	0.87- j2.34	1.52—j2.34	2.32—j2.34	35 + j85	47 + j65	49 + j45	1.49	1.12	1.03
	2% reactive	0.87 -j4.68	1.52—j4.68	2.32—j4.68	9 + j45	14 + j42	19 + j37	3.55	2.59	2.04

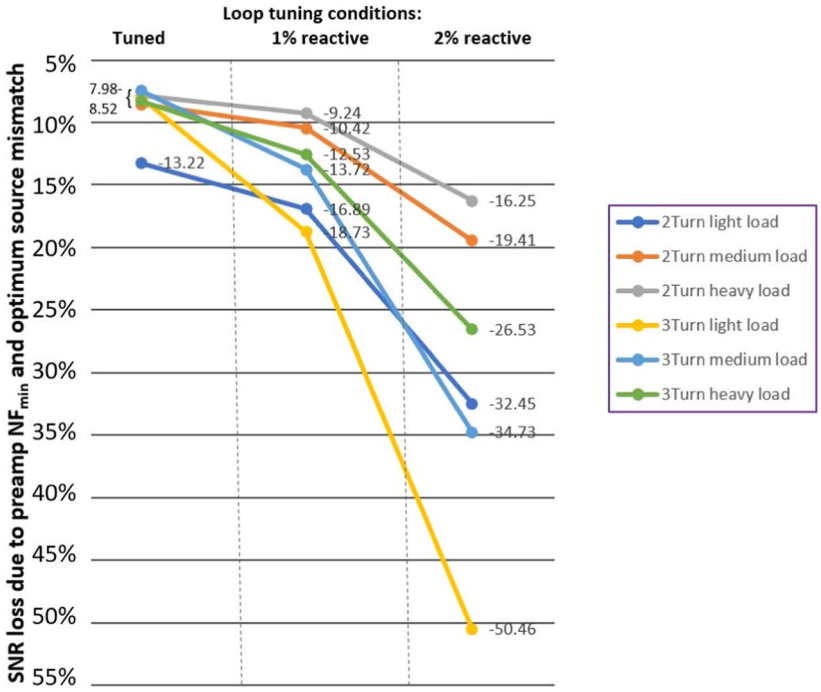

Figure 8. Model of SNR lost with 2 and 3 turn loops (data in table 2).

4.5. Construction and test of the arrays

4.5.1. Electronics and loops

As the results from the loop testing indicated, the two-turn loop exhibited superior *Q* ratios to the single turn and was close to the 3 turn when moderately loaded. Noise figure penalties for the 2- and 3-turn loops were essentially the same for tuned, medium and heavy loading, although higher with the 2-turn lightly loaded case.

Preamplifier blocking values were improved from ~37 Ω with the WMA08HA preamplifier to 90 Ω with the WMA08HB, but stability concerns with the WMA08HB preclude its use as currently implemented. Therefore, the WMA08HA preamplifier was utilized in the array coils. It is expected that our preamplifier blocking requirement will increase with the number of turns (N) squared and we are already short of our design goal for blocking impedance of 100 Ω. Therefore, 2-turn loops were chosen for the array coils.

Given the inductance of the two-turn loop at 2.04 uH, a medium loaded loop resistance at ~0.75 Ω, and the poor, 37 Ω, preamplifier blocking, equation (4), would indicate we need to control the coupling coefficient, k_m, to ~0.022 for a 10% SNR loss, more stringent than the k_m~0.034 for 10% signal coupling from equation (1).

Following an earlier array coil prototype, posterior loops were created in an ~206 cm^2 octagon shape. We found no particular advantage with the octagon, therefore we utilized circular loops of the approximate same area for the anterior. Attempts to add the third loop in a several-cm underlapped position (not at a mutual inductance minimum) showed large impacts on the diagonal neighbour's unloaded *Q*, reducing it by more than 3-fold and demonstrating that preamplifier blocking was inadequate with the closely spaced, underlapped coils. Moving to a more critical overlap with its diagonal neighbour creates few coupling issues with its adjacent neighbours. Therefore, three coils were placed into 3 overlapped loops in a triangular pattern as depicted in figure 10(a), to rely on more critical overlaps, reducing the mutual inductance between the 3 coils in each of the two half arrays. Approximately 3.0 cm to 4.0 cm overlaps were experimentally found to achieve their best isolation in both the posterior and anterior arrays.

Each array coil was stimulated in the same way, and data was gathered indicating the sensitivities at 8.5 MHz and the isolation between stimulated and un-stimulated coils. In figure 10(a), the data indicates sensitivities are close to one another (<2 dB between all channels). Isolation across elements of the posterior and anterior arrays are in excess of 20 dB (less than 10% coupling). Figure 10(b) shows test data indicating that about 15 cm of separation is required to achieve 20 dB of isolation between the posterior and anterior coils when centered over each other, consistent with our model with the modest blocking impedance of 37 Ω (see figure 10(b)).

4.6. Mechanical packaging

The loops and interface electronics were taped onto a soft urethane foam pad of approximately 2 cm thickness for the posterior array (figure 11(a)), and onto a thin polyethylene sheet for the anterior array (figure 11(b)).

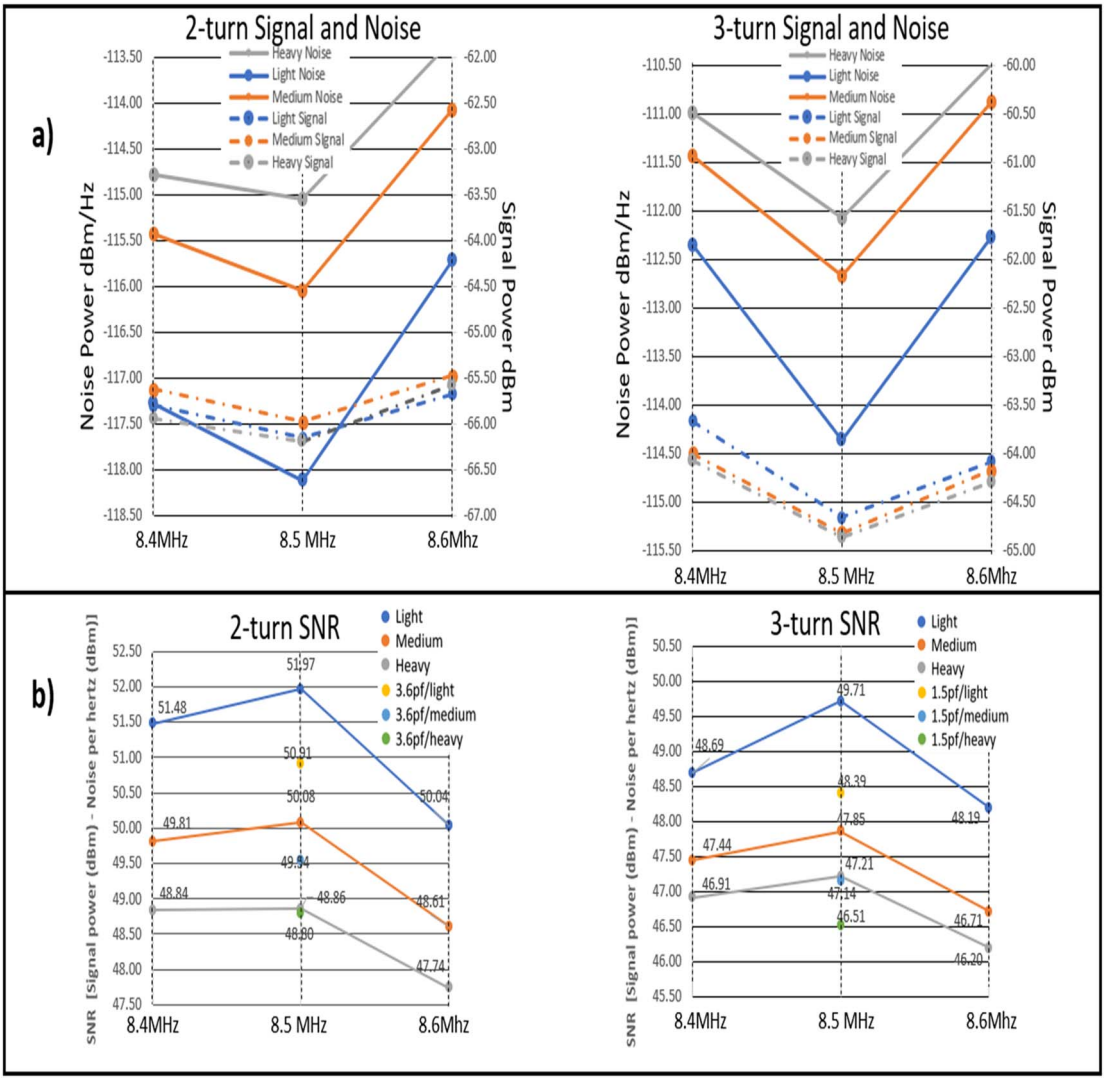

Figure 9. (a) 2-turn and 3-turn coil noise and signal data with light, medium, and heavy loading @ 8.4, 8.5, and 8.6 MHz. and at 8.5 MHz with a 2% reactance change. (b) 2-turn and 3-turn coil noise and signal data with light, medium, and heavy loading @ 8.4, 8.5, and 8.6 MHz and repeated at 8.5 MHz with a 2% reactance change.

Finally, the arrays were enclosed with a flexible cover over the posterior array (figure 11(c)), and in a cast urethane textile bag with an internal, ~7 mm fabric padding over the anterior array (figure 11(d)). Finally, a typical application of the array is shown in figure 11(e).

4.7. Imaging results

Volunteer imaging has commenced with the array, and it has been utilized for studies of kidneys, heart, and rectum. Figure 12 is of a healthy volunteer, lower torso image with the 6 individual elements of the array coil images displayed, figure 12(a), as well as the sum-of-squares combined image, figure 12(b). The system's whole-body transmit coil does not have receive capability, so no comparative study could be performed between the large volume coil and the array.

5. Discussion

The low loss of ultra-fine litz wire appears to be of benefit over traditional wire at 8.5 MHz. Further improvements over the 1600-strand 1.50 mm stranded bundle we used may be possible in the future as suppliers offer finer and finer stranding bundles and optimization for high frequencies. Litz wire is inherently flexible and, based on our experience, surprisingly durable. However, it is noted that terminating and protecting the wire bundles does require particular care.

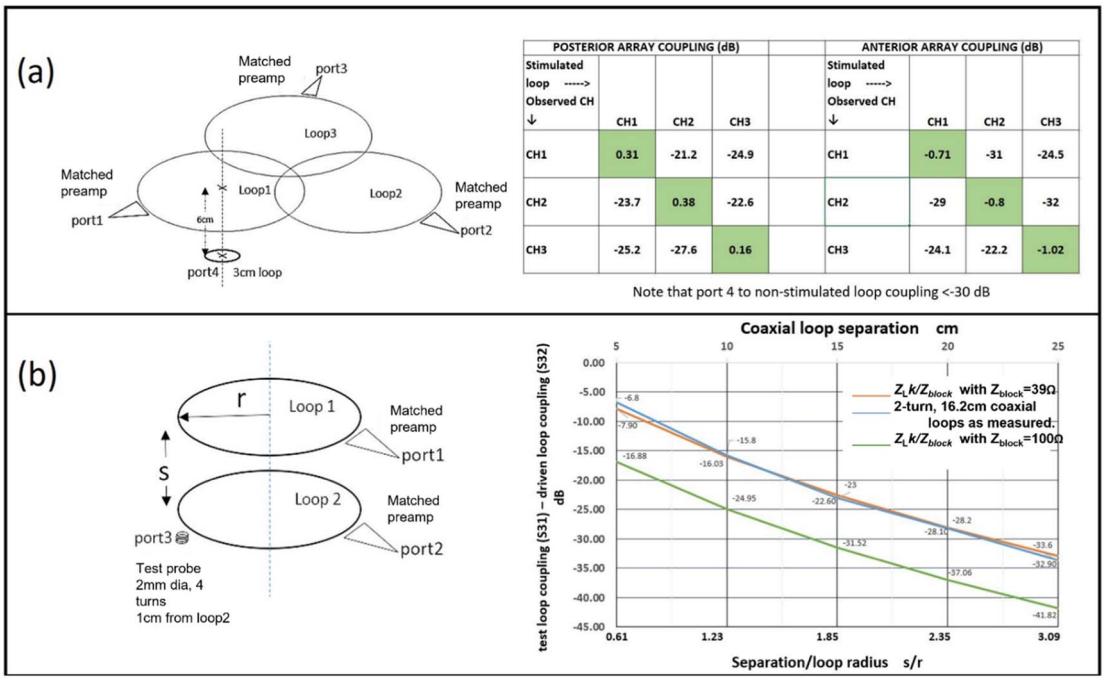

Figure 10. (a) Coplanar coil isolation results for the anterior and posterior arrays. (b) Coaxial coil test results and model.

Multi-turn loops create some mechanical and construction challenges. The desired *Q* ratio improvements will be less than the theoretical values as proximity effects and inter-turn capacitances erode some of the benefit. Additionally, mutual inductance increases demand for higher blocking performance when these coils are incorporated in an array. However, to operate in the body dominated region of our *%SNR* versus a lossless loop curve (figure 5), higher turn count loops do have potential for an adaptable array.

The WMA08HA based electronics feed-board performs well, except that preamplifier blocking was only about one third of our design goal. This is evident in both the co-planar and coaxial coil interactions observed. The WMA08HB has potential to improve our coil-to-coil isolation by about 10 dB, and efforts are underway to stabilize that design. We managed to control the co-planar coil interactions by selecting a 3-loop layout with critical overlaps, but coaxial (anterior to posterior) interactions do not have that option and our desire to improve preamplifier blocking remains. It is possible to improve the preamplifier decoupling by increasing the characteristic impedance of the inverter circuit. For example, it can be improved 3-fold by increasing the 14 Ω inverter impedance by $\sqrt{3}$ (to about 24 Ω). However, this same inverter will present 3-times higher impedances to the preamplifier, moving performance away from the <1.0 dB *NF* goal. This overmatching of the preamplifier may still be a reasonable tradeoff as coupling noise may be higher than *NF* penalties from the mismatch. It should also be noted that the nature of the highly mismatched (low input impedance relative to source impedance) decoupling preamplifier is a linear reduction in power gain as the source impedance moves higher and higher. A 3-fold increase in the source resistance presented to the preamplifier will lower the gain by almost 5 dB and risk having insufficient gain to overcome the losses and *NF* of the receive chain. Therefore, our efforts have focused on improving the preamplifier input impedance.

We have chosen to have the preamplifier decoupling real, and then assess its impact on coupled loops' Q degradation. Our arrangement also, under the tuned conditions, presents a mostly real impedance to the preamplifier where its optimal Noise figure is located. The question has been raised whether reactive preamplifier decoupling could reduce the losses being added to coupled loops; this is a good topic for future study.

SNR test data may indicate some tuning issues with the method employed, which was to open the coil preamplifier interface and tune the coil for a real source impedance. The SNR values were highest at the central frequency in each case, but the SNR decreases were not very symmetrical about 8.5 MHz at 8.4 MHz and 8.6 MHz.

Referring to figure 9, the lightly loaded 3-turn coil has very similar noise power to the heavily loaded 2-turn as would be expected since they present about the same source impedance to the preamplifier. However, the signal with the lightly loaded 3-turn is expected to be about 3.5 dB higher 20 log (3/2) and therefore the SNR

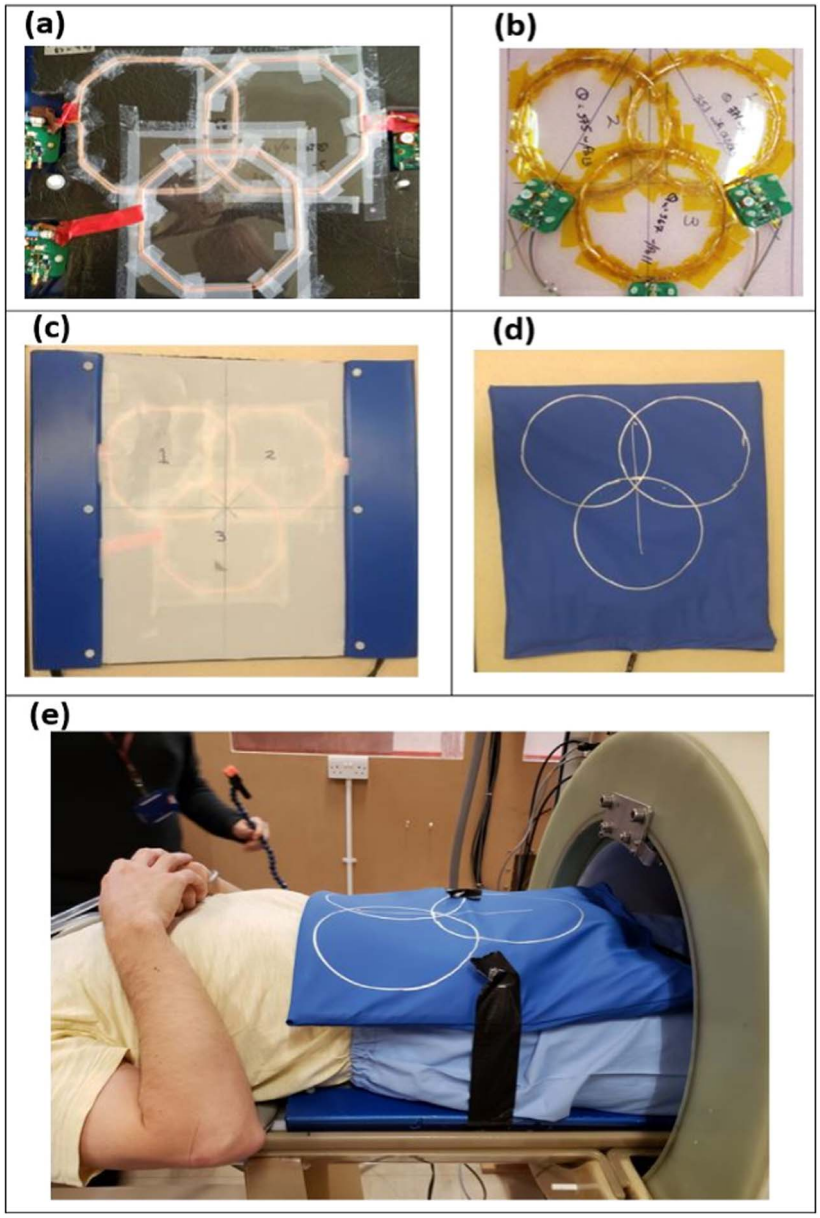

Figure 11. (a) Posterior loops as constructed, (b) anterior loops as constructed. (c) packaged posterior array. (d) packaged anterior array. (e) typical placement of the anterior and posterior arrays.

similarly higher, yet we see <1 dB advantage. Since it is a signal deficit versus a noise increase, possible explanations could be a set-up of the probe distance to the loop, or some interaction with the higher inductance 3-turn loop and the test system.

SNR with loading trends as expected, the flat signal level with loading variations is understood since the available signal power from the source should change linearly with load resistance, but the gain of the preamplifier is changing roughly as the inverse of the load resistance. Also, the decreasing noise power and increasing SNR with decreasing loads is expected as the available noise power is not a function of loading (noise power = kTB), yet the power gain of the preamplifier is decreasing, roughly proportional to the inverse of the source impedance.

Loop losses, under normal loaded and tuned conditions, should cause the largest SNR penalty. However, electronic noise from the interfaced preamplifier can exceed loop losses under some loading and tuning conditions. From figure 8, with a lightly loaded 2-turn loop and 1% reactive mistuning, an approximate 6% SNR penalty is added due to the higher preamplifier *NF*, but it may be possible to tune the loops low in frequency, keeping the source inside a better noise circle as the loops are distorted.

Studies of various sized loops and quadrature combined butterfly elements are underway and may provide improved coverage and/or SNR versus the 3 element, 16.2 cm anterior and posterior array.

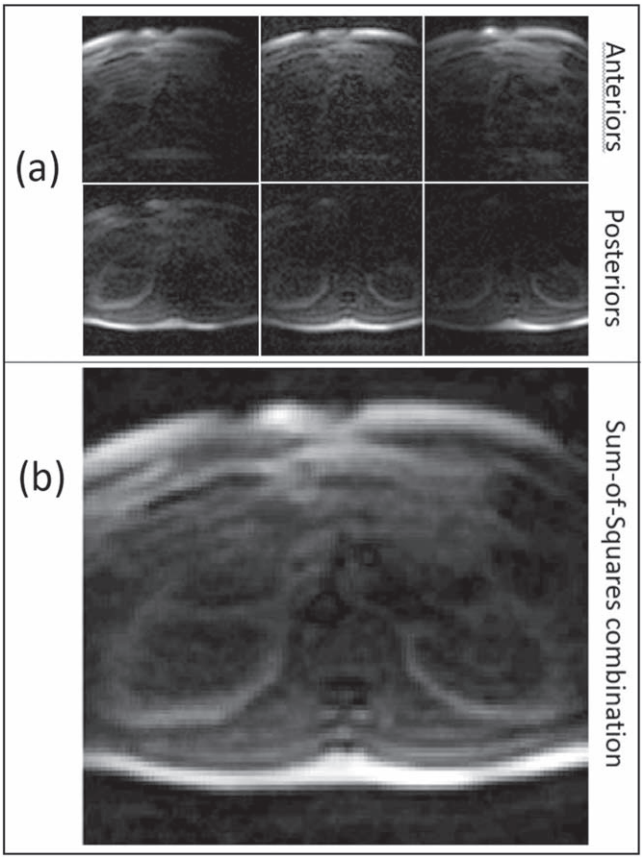

Figure 12. Healthy volunteer image of kidneys, with scan parameters: 0.2 T read-out, Spin-Echo, Matrix size = 64 × 64, Acquisition Bandwidth = 25 kHz, FOV = 400 mm, TE = 19 ms, Slice thickness = 10 mm. (a) Individual array element images. (b) Sum-of-squares reconstruction.

6. Conclusion

Our packaged posterior and anterior arrays are comfortable, very easy to apply, and the coil is being received well by scan volunteers. Image quality continues to improve as various scanner subsystems evolve, pulse sequences are optimized, and post processing and reconstruction methods are evaluated.

Because of the relatively poor blocking impedance, we were constrained to critical overlaps on each array and require a full loop diameter spacing between the anterior and posterior coils to meet our noise and signal coupling targets. Our goal remains to rely heavily on preamplifier decoupling to form truly adaptable, conforming arrays and we continue to work to improve in this area.

Litz wire is showing measurable loss improvements over similar diameter solid wire at 8.5 MHz and the flexibility makes its use extremely compatible with adaptable arrays.

Data availability statement

All data that support the findings of this study are included within the article (and any supplementary information files). Data will be available from 2 February 2023.

Ethical statement

The included image of a healthy volunteer was made as part of an ongoing study for kidney imaging, which was approved by the North of Scotland Research Ethics Committee (REC reference (Sánchez-Heredia *et al* 2019)/ NS/0096). The research was conducted in accordance with the principles embodied in the Declaration of Helsinki and in accordance with local statutory requirements.

ORCID iDs

Lionel M Broche https://orcid.org/0000-0002-8452-9838

References

Bakalski W, Simburger W, Knapp H, Wohlmuth H D and Scholtz A L 2002 Lumped and distributed lattice-type LC-baluns *2002 IEEE MTT-S Int. Microwave Symp. Digest (Cat No02CH37278)* (Seattle, WA, USA: IEEE) pp 209–12

Bracanovic D, Esmail A, Penn S, Webb S, Button T and Alford N 2001 Surface $YBa_2Cu_3O_7$ receive coils for low field MRI *IEEE-TRANSACTIONS ON APPLIED SUPERCONDUCTIVITY* **11** 2422–4

Broche L M, Ross P J, Davies G R, MacLeod M J and Lurie D J 2019 A whole-body fast field-cycling scanner for clinical molecular imaging studies *Sci. Rep.* **9** 10402

Gabriel S M, Lau R W and Gabriel C 1996 The dielectric properties of biological tissues: II. Measurements in the frequency range 10 Hz to 20 GHz *Phys. Med. Biol.* **11** 2251–69

Gilbert K m, Scholl T j and Chronik B a R F 2008 coil loading measurements between 1 and 50 MHz to guide field-cycled MRI system design *Concepts Magn. Reson. B* **33B** 177–91

Giovannetti G 2014 Multiturn surface coil: theoretical considerations on unloaded to loaded Q ratio and SNR *Concepts Magn. Reson. B* **44** 27–31

Giovannetti G and Menichetti L 2017 Litz wire RF coils for low frequency NMR applications *Measurement* **110** 116–20

Gonzalez G 1996 *Microwave Transistor Amplifiers Analysis and Design* (Upper Saddle River, New Jersey. USA: Prentice-Hall, Inc) 2nd978-0-13-254335-4

Grafendorfer T, Conolly S, Matter N, Pauly J and Scott G 2006 Optimized Litz coil design for prepolarized extremity MRI *14th SCIENTIFIC MEETING & EXHIBITION of the ISMRM Seattle WA. USA* **1** 2613

Hoult D I and Richards R E 2011 The signal-to-noise ratio of the nuclear magnetic resonance experiment *J. Magn. Reson.* **213** 329–43

Izadian A 2019 *Fundamentals of Modern Electric Circuit Analysis and Filter Synthesis.* (Berlin: Springer)

Kato H *et al* 2005 Composition of MRI phantom equivalent to human tissues *Med. Phys.* **32** 3199–208

Kumar A, Edelstein W A and Bottomley P A 2009 Noise figure limits for circular loop MR coils *Magn. Reson. Med.* **61** 1201–9

Landau L D and Lifshitz E M 1984 *Chapter VII—Quasi-Static Electromagnetic Field* ed L D Landau and E M Lifshitz 2nd ed (Amsterdam: Pergamon: Electrodynamics of Continuous Media) pp 199–224

Lee R F, Giaquinto R O and Hardy C J 2002 Coupling and decoupling theory and its application to the MRI phased array *Magn. Reson. Med.* **48** 203–13

Lurie D J *et al* 2010 Fast field-cycling magnetic resonance imaging *Multiscale NMR Relax* **11** 136–48

Ma Q Y *et al* 2003 Superconducting RF coils for clinical MR imaging at low field1 *Acad. Radiol.* **10** 978–87

Pettai R 1984 *Noise in Receiving Systems.* (New York: Wiley)

Redpath T 1998 Signal-to-noise ratio in MRI *Br. J. Radiol.* **71** 704–7

Reese B A, Joseph R and Sullivan C R 2018 Improved litz-wire designs for the MHz range *2018 IEEE 19th Workshop Control Model Power Electron COMPEL; 1–8*

Roemer P B, Edelstein W A, Hayes C E, Souza S P and Mueller O M 1990 The NMR phased array *Magn. Reson. Med.* **16** 192–225

Rosa E B and Grover F W 1916 Formulas and tables for the calculation of mutual and self-inductance (Revised) *Bulletin of the Bureau of Standards* **8** 1No 169

Russell K J and Carter D J 2019 NANO-LITZ The Charles Stark Draper Laboratory Article AD1088727 (https://apps.dtic.mil/sti/citations/AD1088727)

Sánchez-Heredia J D *et al* 2019 Improved decoupling for low frequency MRI arrays using non-conventional preamplifier impedance *IEEE Trans. Biomed. Eng.* **66** 1940–8

Smith G S 1972 Proximity effect in systems of parallel conductors *J. Appl. Phys.* **43** 2196–203

Sullivan C R 1999 Optimal choice for number of strands in a litz-wire transformer winding *IEEE Trans. Power Electron.* **14** 283–91

Terman F E 1943 *Radio Engineer's Handbook* (New York, NY. USA: McGraw-Hill.) 1st2 37 (https://books.google.com/books?id=b7Q8AAAAIAAJ) 0070636303

UK Stroke Forum Abstracts 2018 *Int. J. Stroke* **13** 10–65

Vaughan J T and Griffiths J 2012 Quadrature Surface Coils *RF Coils for MRI* (New York: Wiley) 1st3 19978-0-470-77076-4